



Doping effect of alkali metal elements on the structural stability and transport properties of ZnO at high pressures

HPSTAR
595-2018



R. Thiyagarajan^a, Xiaozhi Yan^a, V. Pazhanivelu^b, A. Paul Blessington Selvadurai^b,
R. Murugraj^b, Wenge Yang^{a, c, *}

^a Center for High Pressure Science and Technology Advanced Research (HPSTAR), Shanghai 201203, PR China

^b Department of Physics, Anna University (MIT Campus), Chennai 600044, India

^c High Pressure Synergetic Consortium (HPSynC), Geophysical Laboratory, Carnegie Institution, Argonne, IL 60439, USA

ARTICLE INFO

Article history:

Received 15 September 2017

Received in revised form

4 March 2018

Accepted 2 April 2018

Available online 4 April 2018

Keywords:

Semiconductor

Phase transition

High-pressure

Synchrotron x-ray diffraction

ABSTRACT

In this paper, we report the tuning effects on the structural stability and transport properties of ZnO under high pressure at room temperature after doping it with a series of alkali metal elements (Li, Na, and K). Generally, substitution at the Zn site (with the large ionic radii of the 1st group elements) leads to *p*-type conductivity with an increase in the Zn–O bond distance. Whereas, the external high pressure compresses the crystallite size, leading to increased lattice strain and band gap reduction in this semiconductor material. As a result of lattice strain hindrance upon compression, the larger ions rather than the smaller ions try to counteract the high pressure due to ionic force repulsion within the lattice. By combining synchrotron x-ray diffraction, Raman spectroscopy and *in situ* resistance measurements under pressure on Li-, Na-, and K-doped ZnO nanomaterials, we demonstrated that the critical phase transition pressure of ZnO from wurtzite to rock salt changes from 9 GPa to 13 GPa, and a resistance change anomaly occurs around these transition pressures. This study of the structural, vibrational stability and transport properties of a series of alkali metal element-doped ZnO under pressure provides an efficient way to modify these types of semiconductor materials for technological applications.

Published by Elsevier B.V.

1. Introduction

ZnO has gained much research interest due to its unique properties and wide spread applications. It is a wide and direct band gap material (3.32 eV) with a large excitonic binding energy of 60 meV. It appears in three different crystal structures; a hexagonal wurtzite structure, zinc blende structure and rock salt phase, but the wurtzite structure only appears under normal conditions. ZnO has potential applications in LEDs, sensors, solar cells and spintronic device fabrication. The sintering and doping processes decide the basic properties and potential applications of ZnO [1].

The structural stability and phase transformation of materials have been extensively studied in the fields of materials science, condensed matter physics, geophysics and industrial engineering [2–4]. Moreover, the mechanism of pressure-induced phase transitions have been widely investigated ranging from studies on the

Earth's interior dynamics to multifunctional materials with tailored properties [5–7]. During a pressure-induced phase transition, structural impurities including defects, voids, dislocations, stacking faults, and twinning play vital roles in material deformation, nucleation, and growth. These impurity factors can be reduced by decreasing the particle size [8,9]. Generally, bulk crystals are often structurally imperfect while nanocrystals are considered defect-free [10], thus nanomaterials are considered to be more stable than their bulk counterparts. During the nucleation of a new phase, multiple domains often take part in bulk samples, whereas only a single nucleation domain participates in nanocrystals [8,9]. The surface area increase in nanocrystals produces a higher surface energy than bulk materials, which alters both their phase transition routes and onset transition pressures.

Several groups have individually claimed a pressure-tuned structural transition in conventional ZnO-diluted semiconductor materials. Initially, Saitta et al. [11] and Boulfelfel et al. [12] theoretically predicted a wurtzite to rock salt phase transition, which was later confirmed experimentally at 9 GPa during compression measurements [13]. Kumar et al. [14] studied the pressure-induced

* Corresponding author. Center for High Pressure Science and Technology Advanced Research (HPSTAR), Shanghai 201203, PR China.

E-mail address: yangwg@hpstar.ac.cn (W. Yang).

structural transition of ZnO in both its nano and bulk crystal forms. The structural transition of their nanocrystalline sample occurred at 10.5 GPa, which was 1.5 GPa higher than the bulk form. This type of difference in the transition pressure has also been confirmed in other nanomaterials like Si, CdSe, CdS, PbS, ZnS, and Fe₂O₃ [3,15–19]. Moreover, the coexistence of rock salt and wurtzite phases was observed in nanosize samples too [14] and confirmed by Raman scattering experiments under high pressure [20]. The wurtzite to cubic transformation in ZnO nanowires begins at 9 GPa and completes at 13.8 GPa [21]. Chen et al. studied the pressure effect on ZnO photoluminescence and reported an enhancement of the direct band gap energy within the wurtzite structure [22,23]. The same structural transition was also observed at 11.3 GPa by ZnO electrical resistance measurements [24]. An internal perturbation such as doping is one of the most effective ways of controlling the structure and properties of ZnO [3,15–19]. The pressure required to trigger a phase transition in the Mn-doped ZnO system (Zn_{0.98}Mn_{0.02}O) was lowered from 9.5 GPa to 6.5 GPa [25,26]. Bouibes and Zaoui theoretically analyzed the high-pressure stability of ZnO with an *ab initio* evolutionary algorithm using the USPEX code and confirmed the predicted wurtzite to cubic phase transition at 10.45 GPa [27].

Recently, Pazhanivelu et al. reported unexpected ferromagnetism in pure and 1st group element-doped ZnO nanoparticles [28]. The doping elements occupied the interstitial sites rather than the substitution sites, with partial migration of their small atomic radii, and therefore acted mainly as donors. Furthermore, doping with a series of 1st group elements with increasing ionic radii lead to a simultaneous change in bond length, where the ZnO lattice size and structural stability under high pressure were largely affected by doping. In this paper, we report our systematic investigations on the structural, vibrational, and resistivity properties of selected samples under pressure to explore the effect of pressure that leads to a structural transition and its dependence on the ionic radii of the substitution elements in ZnO.

2. Experimental details

Pure ZnO and 1st group element-doped nanoparticles (Zn_{0.95}Li_{0.05}O, Zn_{0.95}Na_{0.05}O, and Zn_{0.95}K_{0.05}O) were prepared using a co-precipitation method [28]. The starting reagent materials were zinc acetate, 1st group elements acetates and oxalic acid. Initially, we dissolved the acetates and oxalic acid in deionized water in a 0.4 M solution with a ratio of 1:1. Then, the mixed solution was stirred continuously for 3 h and kept undisturbed overnight to precipitate. The collected precipitates were centrifuged several times with intermediate washing with deionized water and acetone, respectively, and the samples were dried at room temperature for 24 h. Finally, the end product was sintered at 350 °C for 6 h in an open atmosphere. The nanocrystalline phases were confirmed by a Bruker D2 phaser XRD diffractometer with a Cu K_α line and a wavelength of 1.54 Å [28].

Hydrostatic pressure up to ~20 GPa was generated using a symmetrical diamond anvil cell with a pair of 300 micron diamond anvils. The stainless steel T301 gasket was pre-indented to 40–45 μm thick and a hole of 120–150 μm in diameter was laser-drilled in the indented region to form the sample chamber. The prepared ZnO and 1st group element-doped ZnO nanopowders were pre-compressed to pellets, and loaded into the chambers with a small ruby ball. Neon gas and silicone oil were used as the pressure-transmitting media for the XRD and Raman scattering experiments, respectively. The *in situ* high-pressure x-ray diffraction (XRD) experiments were carried out at the 16BM-D beam line, High Pressure Collaborative Access Team (HPCAT) at the Advanced Photon Source (APS), Argonne National Laboratory, with a

wavelength of 0.3101 Å. The diffraction data were recorded with a two-dimensional area detector Mar 345 image plate, then the Fit2D program was used to integrate one-dimensional profiles for structural refinement using the GSAS program [30,31]. *In situ* high-pressure Raman spectra were taken at HPSTAR by a Raman spectrometer (Renishaw) with a 532 nm excitation laser. In both *in situ* high-pressure studies, the pressures applied on the samples were determined by the ruby fluorescence method [32].

3. Results and discussion

3.1. Morphological studies of pristine nanoparticles

Surface morphology measurements of the prepared nanoparticles were carried out using high-resolution scanning electron microscopy (SEM). The SEM micrographs of ZnO, Zn_{0.95}Li_{0.05}O, Zn_{0.95}Na_{0.05}O, and Zn_{0.95}K_{0.05}O are shown in Fig. 1(a)–(d). All the synthesized nanoparticles exhibit a poly-dispersed irregular spherical morphology. In general, the shape and size of nanomaterials are determined by a combination of kinetic and thermodynamic effects. The surface morphology and dimensions of the synthesized particles strongly depend on reaction conditions such as the initial concentration of the precursors, molar ratio, temperature, and *pH* of the solution. Therefore, the size or shape of the compounds can be easily tuned by controlling these experimental conditions. In our preparation process, ZnO nuclei were generated via a reaction between Zn²⁺ and O²⁻ in a solution. The freshly formed nuclei of ZnO tend to grow into larger particles. However, the growth rates of the various faces of the nanoparticles can be kinetically controlled by selective adsorption and desorption on their surfaces. This phenomenon is explained by the Ostwald ripening process, where larger particles grow at the expense of smaller particles. Reduction in the surface energy is the primary driving force for grain growth and morphological evolution [33]. The doping 1st group elements such as Li, Na, and K with ZnO nanoparticles decreases the surface free energy through segregation, allowing segregated atoms to move to the surface and smaller grains to agglomerate. The incorporation of 1st group elements in the ZnO host material increased grain agglomeration.

Transmission electron microscopy (TEM) images were used to confirm the formation of the pure and Li, Na, and K-doped ZnO samples as shown in Fig. 2(a)–(d). In general, the shape-controlled synthesis of nanoparticles is a kinetically controlled process, where low-energy facets are maintained while high-energy facets are destroyed, leading to the formation of a particular subsequent shape enclosed by low-energy planes. Doped synthesis materials have different morphologies because the dopant may preferentially adsorb on specific crystallographic planes and then change the direction and growth rate of the nanoparticles. The evolution of the shape and size of ZnO was achieved by adding different types of dopant (Li, Na, and K) into the chemical reaction. The surface of the ZnO nanoparticles absorbs the dopant to form Zn – (Li, Na, and K) dopant bonds, which may slow down the facet growth rate. The shape evolved from Zn(OH)₂ to ZnO seeds. When K is doped in the growth process, it retains the high surface energy and spherical shape, whereas the Li- and Na-doped samples tended to reduce the surface energy and form a hexagonal shape. From our TEM images, poly-dispersed and well-defined particles were observed. The pure ZnO and Li and Na-doped ZnO samples exhibited a hexagonal-like shape, whereas the K-doped sample was spherical. A selected area electron diffraction (SAED) pattern confirmed the polycrystalline nature of the sample. Individual diffraction spots reflected the ZnO nanoparticles but no Li, Na, and K nanoparticle reflection planes, suggesting that all the 1st group elements were incorporated in the ZnO lattice.

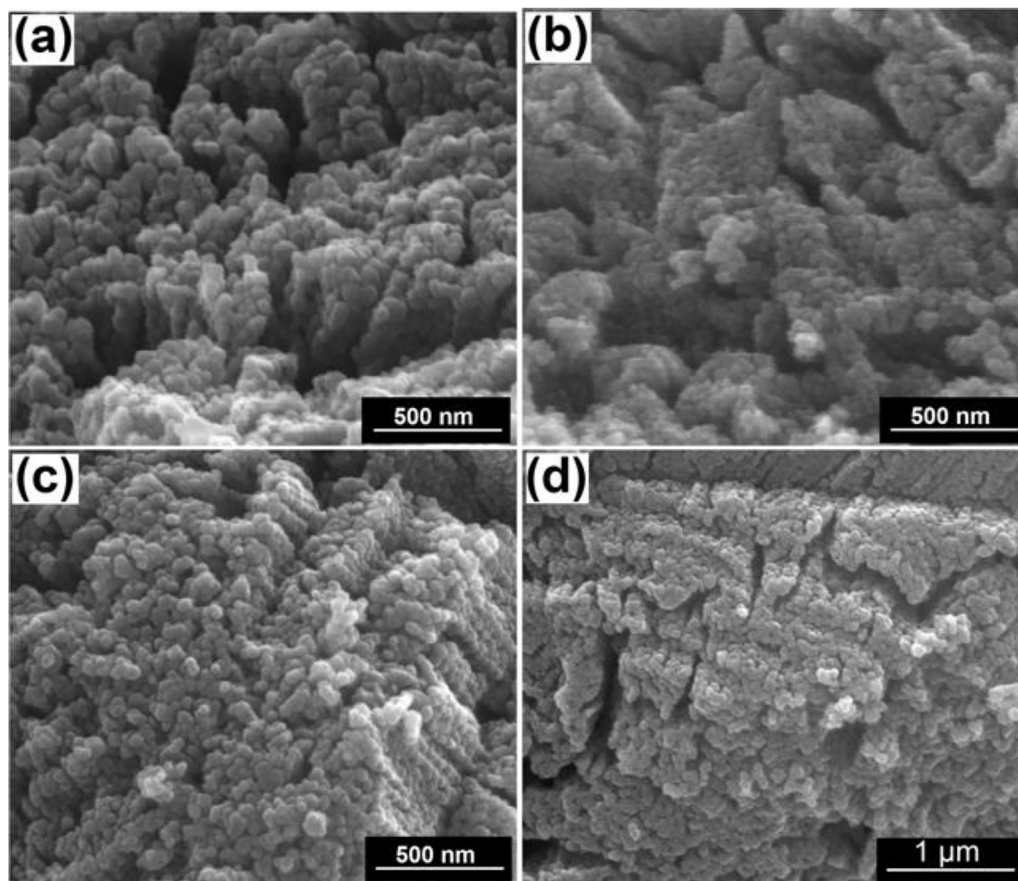


Fig. 1. SEM pictures of the (a) ZnO, (b) $\text{Zn}_{0.95}\text{Li}_{0.05}\text{O}$, (c) $\text{Zn}_{0.95}\text{Na}_{0.05}\text{O}$, and (d) $\text{Zn}_{0.95}\text{K}_{0.05}\text{O}$ samples.

To determine the elemental composition and the percentage of dopant in the ZnO nanoparticles, an appropriate amount of samples were dissolved in nitric acid and de-ionized water and examined by inductively coupled plasma optical emission spectrometry (ICP-MS). The observed compositions are given in Table 1, which shows that the dopant percentages were around 5%, confirming their significant presence in the ZnO lattice. The ICP-MS analysis revealed that the Zn concentration reduces from 61% to 53% with 1st group elements doping. Furthermore, 4.1% of Li atoms, 3.9% of Na atoms, 4.31% of K atoms were incorporated into the interstitial sites rather than the substitution sites, with partial migration of their small atomic radii. Therefore, the dopants acted mainly as donors, compensating the extra electrons arising from the Zn^{2+} interstitials in the prepared ZnO and leaving uncompensated or localized acceptors for room temperature ferromagnetism in these samples [28]. Doping ZnO with 1st group elements stabilized the prepared samples despite their charge neutrality, which is also reflected in previous characterization measurements [28,29]. Of all the dopants, K achieved a higher dopant concentration in the host lattice and induced a morphological variation (as seen in the TEM images).

3.2. High-pressure XRD

The X-ray diffraction patterns of the ZnO, $\text{Zn}_{0.95}\text{Li}_{0.05}\text{O}$, $\text{Zn}_{0.95}\text{Na}_{0.05}\text{O}$ and $\text{Zn}_{0.95}\text{K}_{0.05}\text{O}$ nanoparticles at different pressures up to ~25 GPa are shown in Fig. 3(a)-(d), respectively. The XRD data of the prepared samples were analyzed with GSAS software. At ambient conditions, all the characteristics peaks of the prepared

samples matched a single-phase hexagonal wurtzite structure with space group of $P6_3mc$, which agrees with reported data [28]. As the externally applied pressure increased, a phase transformation from a wurtzite $P6_3mc$ to rock salt Fm-3m phase occurred in all samples, but at different transition pressures. Recently, this phenomenon was theoretically proven by Bouibes and Zaoui using an *ab initio* evolutionary algorithm [27]. The pressure regions for the pure wurtzite, a mixture of the wurtzite and rock salt phases, and the pure rock salt phases are summarized in Table 2 for the ZnO, $\text{Zn}_{0.95}\text{Li}_{0.05}\text{O}$, $\text{Zn}_{0.95}\text{Na}_{0.05}\text{O}$, and $\text{Zn}_{0.95}\text{K}_{0.05}\text{O}$ samples. Table 2 shows that the ZnO transition pressure value increased with 1st group element-doping and with the increasing ionic radii of the substituted 1st group elements.

The strain in each crystal grain of the powder sample and the small grain size effect broadened the XRD peaks. In synchrotron X-ray diffraction, the grain size and strain of diffraction line to width is given as:

$$FWHM^2 \cos^2 \theta = \left(\frac{\lambda}{d} \right)^2 + \sigma \sin^2 \theta$$

where FWHM is the full-width at half-maximum of the diffraction profile on the 2θ scale and the symbols d , λ and σ denote the grain size, X-ray wavelength, and strain, respectively. The estimated values of the crystalline size and lattice strain in both phases of all samples are shown in Fig. 4(a)-(b) as a function of pressure, respectively. From Fig. 4, we observed the following common features for the ZnO, $\text{Zn}_{0.95}\text{Li}_{0.05}\text{O}$, $\text{Zn}_{0.95}\text{Na}_{0.05}\text{O}$, and $\text{Zn}_{0.95}\text{K}_{0.05}\text{O}$ samples: (i) the lattice strain increased with applied external

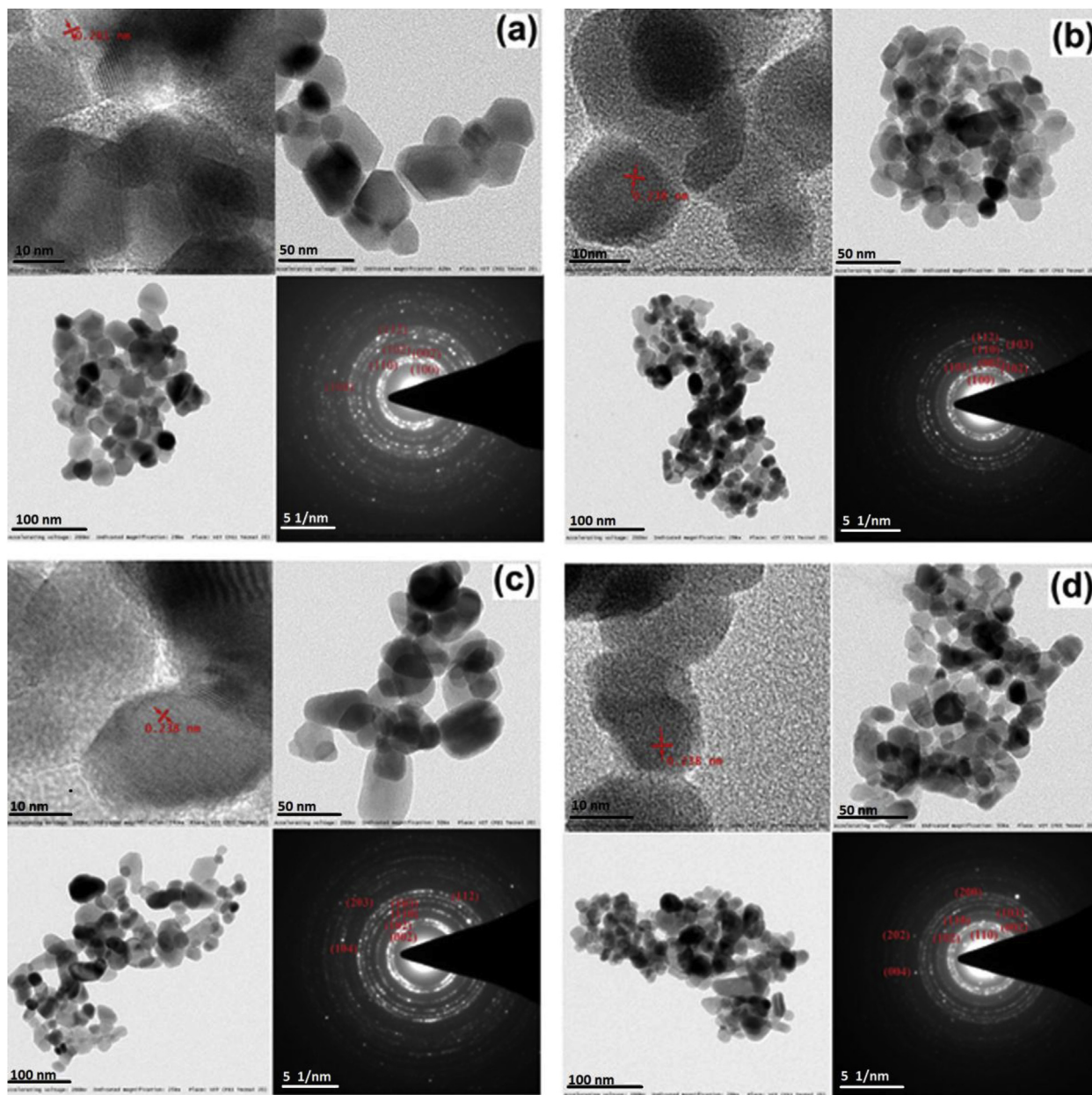


Fig. 2. Micrographs of ZnO (a), Zn_{0.95}Li_{0.05}O (b), Zn_{0.95}Na_{0.05}O (c), and Zn_{0.95}K_{0.05}O (d) samples characterized by TEM. The micrographs at different length scales (panel (i), (ii) and (iii) have a 10, 50, and 100 nm length scale) and corresponding SAED patterns (panel (iv)) for all samples.

Table 1

Observed composition concentration of Zn and 1st group elements with ICP-MS measurements of each sample.

Samples	Zn concentration (%)	Dopant concentration (%)
ZnO	61.78	–
Zn _{0.95} Li _{0.05} O	54.38	4.1
Zn _{0.95} Na _{0.05} O	59.79	3.99
Zn _{0.95} K _{0.05} O	53.65	4.31

pressure in both phases; (ii) the crystalline sizes decreased with applied pressure, both in the hexagonal and cubic phases; and (iii) the doping effects from pure ZnO to K-doped ZnO increase the crystalline size, while strain decreases it.

The pressure dependence of the unit cell volume derived from

the GSAS fittings for both the observed phases are given in Fig. 5(a)–(d) for the four prepared samples. The Birch-Murnaghan (BM) equation of state was fitted to each phase and all their sample data points to estimate the bulk moduli (B_0) and initial volume (V_0) for both the low- and high-pressure phases of the four samples. Fig. 6(a) and (b) show the initial volumes and bulk moduli (B_0) of both phases with respect to the ionic radii. At zero-pressure, the isothermal bulk moduli (B_0) value of the pure ZnO sample is 178 GPa, which agrees with the literature. However, the B_0 values of 1st group element-doped ZnO decreased in both the low-pressure and high-pressure phases.

In general, the phase transition in nanosized particles needs a higher pressure than bulk particles due to the higher surface energy possessed by nanoparticles. Conversely, in our case, the 1st group element-doped ZnO samples had larger unit cell volumes than the

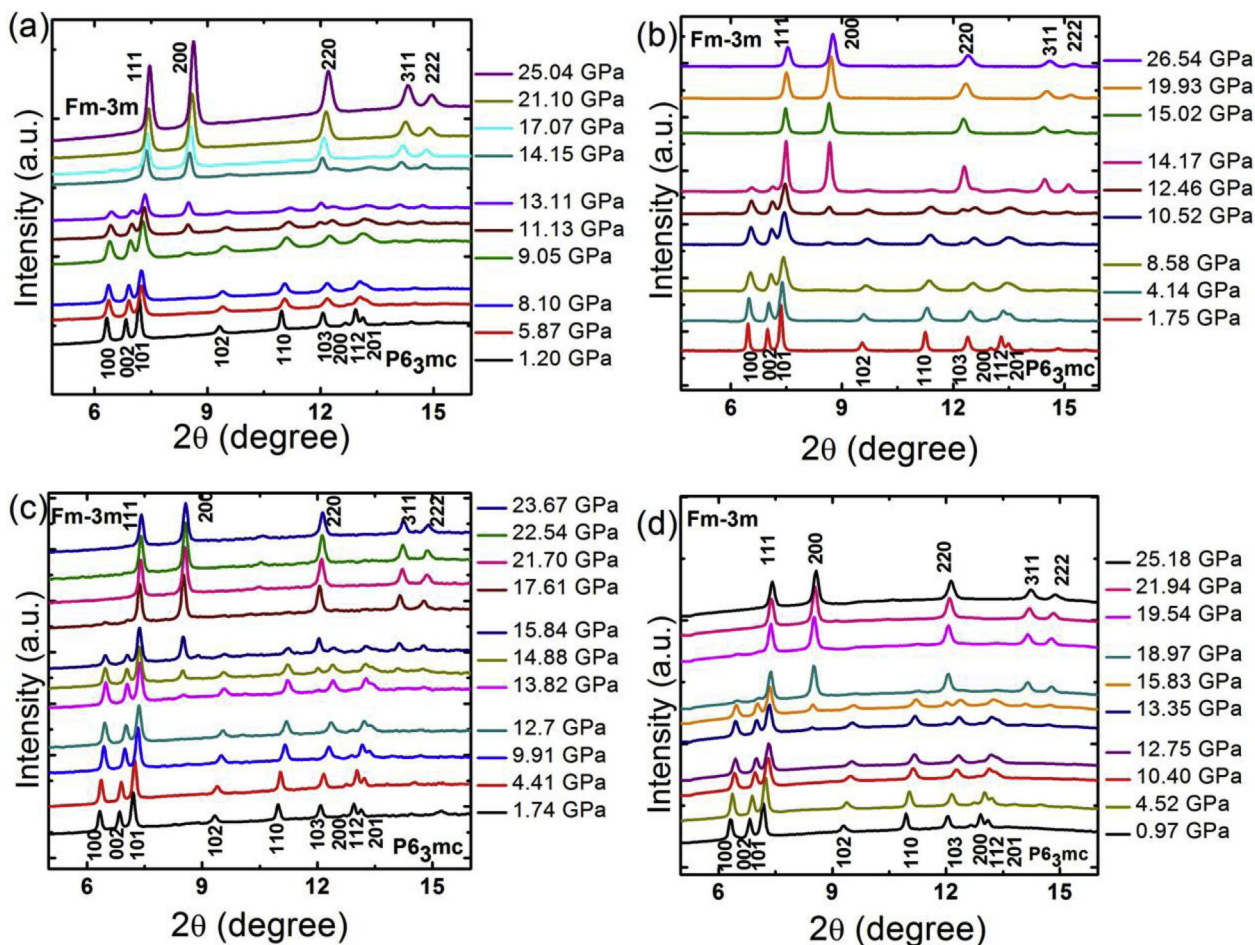


Fig. 3. X-ray diffraction patterns collected at different pressures for the (a) ZnO, (b) $Zn_{0.95}Li_{0.05}O$, (c) $Zn_{0.95}Na_{0.05}O$, and (d) $Zn_{0.95}K_{0.05}O$ samples.

Table 2
Transition pressure values derived from high-pressure XRD data for the start of the rock salt cubic phase, mixed phase region, and end of the wurtzite phase for ZnO, $Zn_{0.95}Li_{0.05}O$, $Zn_{0.95}Na_{0.05}O$, and $Zn_{0.95}K_{0.05}O$.

Samples	Pure wurtzite phase	Start of rock salt cubic phase -end of wurtzite phase	Pure rock salt cubic phase
ZnO	8.10 GPa	9.05–13.11 GPa	14.15 GPa
$Zn_{0.95}Li_{0.05}O$	8.58 GPa	10.52–14.17 GPa	15.02 GPa
$Zn_{0.95}Na_{0.05}O$	12.70 GPa	13.82–15.84 GPa	17.61 GPa
$Zn_{0.95}K_{0.05}O$	12.75 GPa	13.35–18.97 GPa	19.54 GPa

pure ZnO sample. The phase transition pressures were also higher than the pure ZnO sample. The incorporation of 1st group elements in ZnO enhanced its stability, i.e., the wurtzite phase was sustained at higher pressures. The change in the volume percentage from the wurtzite to rock salt phase transition decreased with an increase in the ionic doping elements' radii, as shown in Fig. 6(c), which confirms the counteracting effect of doping with external pressure.

3.3. High-pressure Raman analysis

Raman spectroscopy is a sensitive characterization tool for local bonds, material quality, phase orientation, and the interaction of phonons in samples. The high-pressure Raman spectra of pure and 1st group element-doped ZnO nanoparticles are displayed in Fig. 7(a)–(d). The vibrational modes of wurtzite ZnO are assigned by group theory as $A_1 + 2B_1 + E_1 + 2E_2$. The A_1 , E_1 , and E_2 are active modes, and B_1 is a non-active (forbidden) mode for the pure ZnO

wurtzite structure. The two polar modes are assigned to A_1 and E_1 , which are split further into transverse (TO) and longitudinal (LO) vibration modes. The $2E_2$ modes are related to the lattice vibrations of the Zn atoms and are non-polar modes that act as an E_2 low and E_2 high mode.

In the wurtzite structure there are six vibrational modes, 2 TA(M), $2E_2$, E_2 high, A_1 (TO) and $[2(E_2H - E_2L)]$, at around 210, 350, 436, 570, 680, and 606 cm^{-1} , respectively. As the external pressure increases gradually, the intensity of the E_2 high mode decreases. The E_2 mode is a characteristic vibrational mode of the wurtzite structure, and reflects the structural characteristics of ZnO. Due to doping, the E_2 mode shifts towards a higher wavenumber through strain inducement in the lattice at ambient conditions. In addition, due to the effect of external high pressure, the E_2 high mode moves towards a higher wavenumber and decreases in intensity because of lattice strain and the phase transition, respectively.

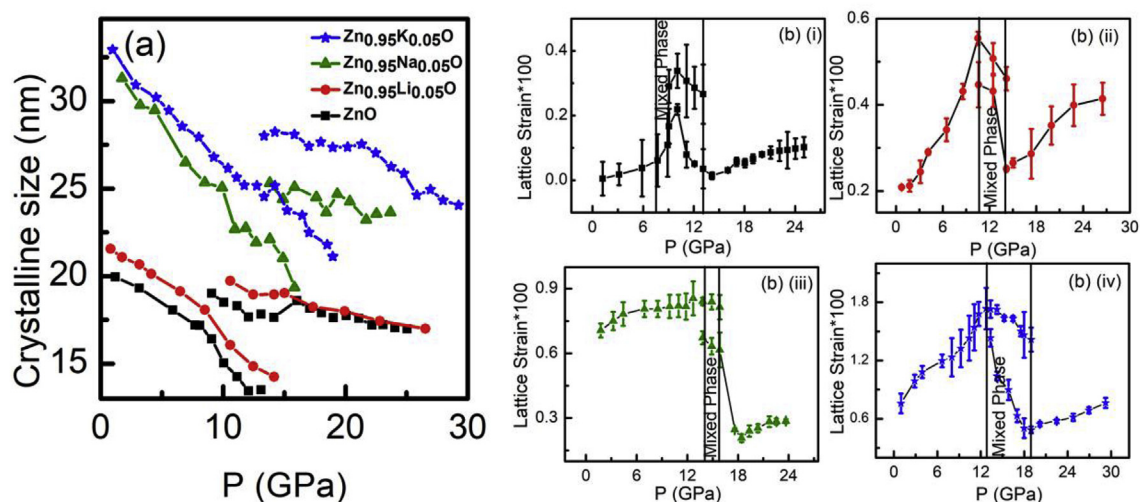


Fig. 4. Pressure effect on the (a) crystalline size and (b) lattice strain of the (i) ZnO, (ii) Zn_{0.95}Li_{0.05}O, (iii) Zn_{0.95}Na_{0.05}O, and (iv) Zn_{0.95}K_{0.05}O samples.

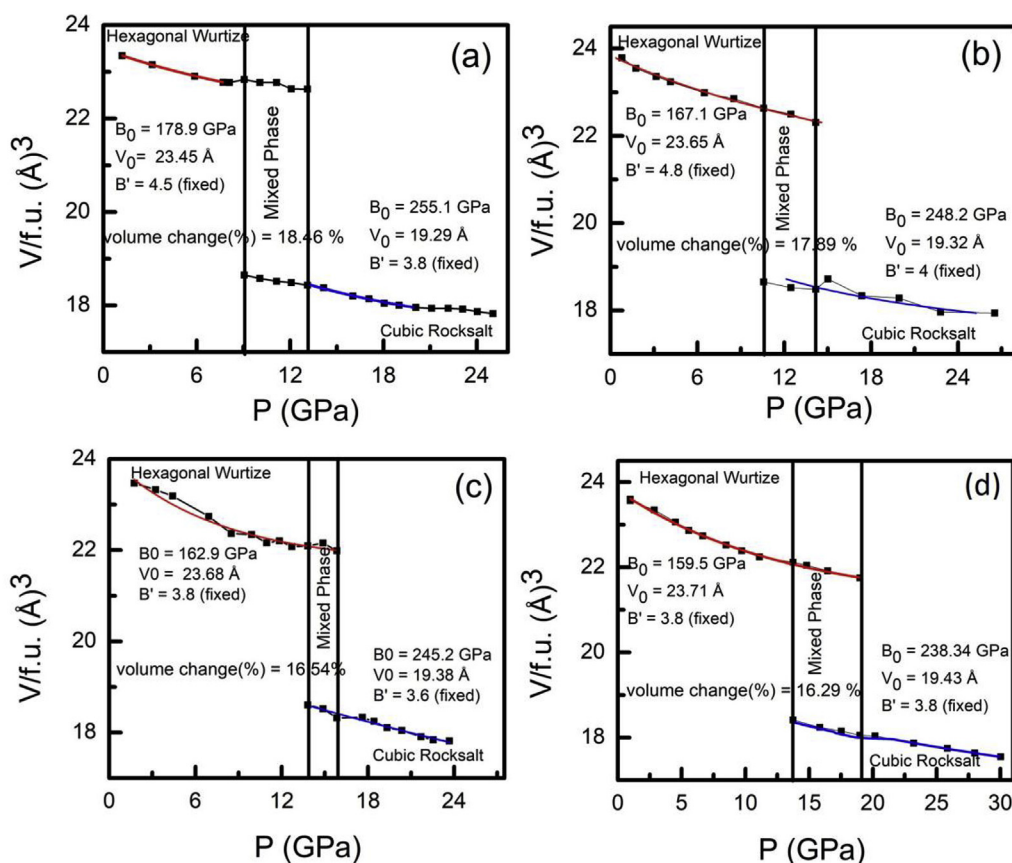


Fig. 5. Volume-pressure equation of state plots for the (a) ZnO, (b) Zn_{0.95}Li_{0.05}O, (c) Zn_{0.95}Na_{0.05}O, and (d) Zn_{0.95}K_{0.05}O samples.

When the structural transition occurs, all the wurtzite vibrational modes vanish and two new broad peaks appear at 140 and 537 cm^{-1} due to intrinsic lattice defects, which are associated with a phase transition at high pressure. This same phenomenon was reported by Xiaoqin Yan et al. [34]. Moreover, new rock salt phase vibrational modes appeared at 9.15, 10.87, 11.28, and 12.53 GPa for the pure, Li-, Na- and K-doped ZnO nanoparticles, respectively. The observed Raman spectra of these samples are shown in Fig. 8(a–d).

The phase transition pressures based on the Raman spectrum analysis on all four ZnO systems are summarized in Table 3, which shows that the transition pressures of the B4 to B1 structures increase with respect to the dopant ion sizes (Li, Na, K) in ZnO. Furthermore, the E2 high mode of the wurtzite phase remains well beyond the transition pressure (12.95, 13.94, 16.27, and 17.39 GPa for the pure, Li-, Na- and K-doped ZnO nanoparticles, respectively) while the other Raman modes of the pure and doped ZnO samples

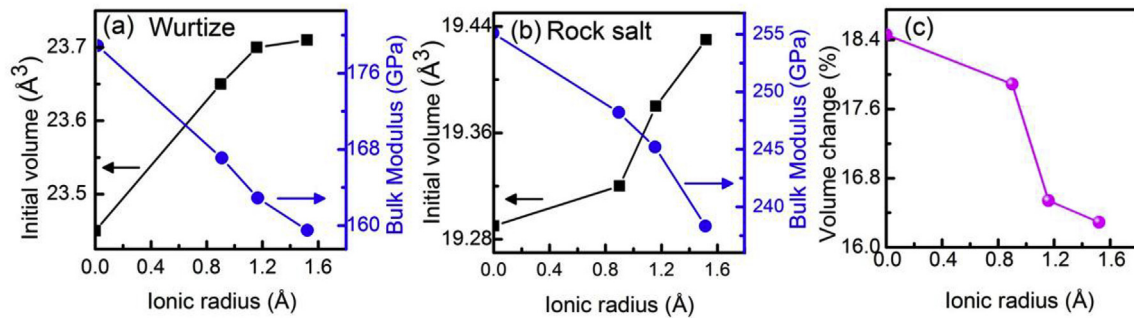


Fig. 6. Initial volume (left axis black squares) and bulk modulus (right axis blue circles) as a function of the doping elements' ionic radii in the (a) wurtzite phase and (b) rock salt phase. (c) Volume collapse at phase transition with different doping elements. (For interpretation of the references to colour in this figure legend, the reader is referred to the Web version of this article.)

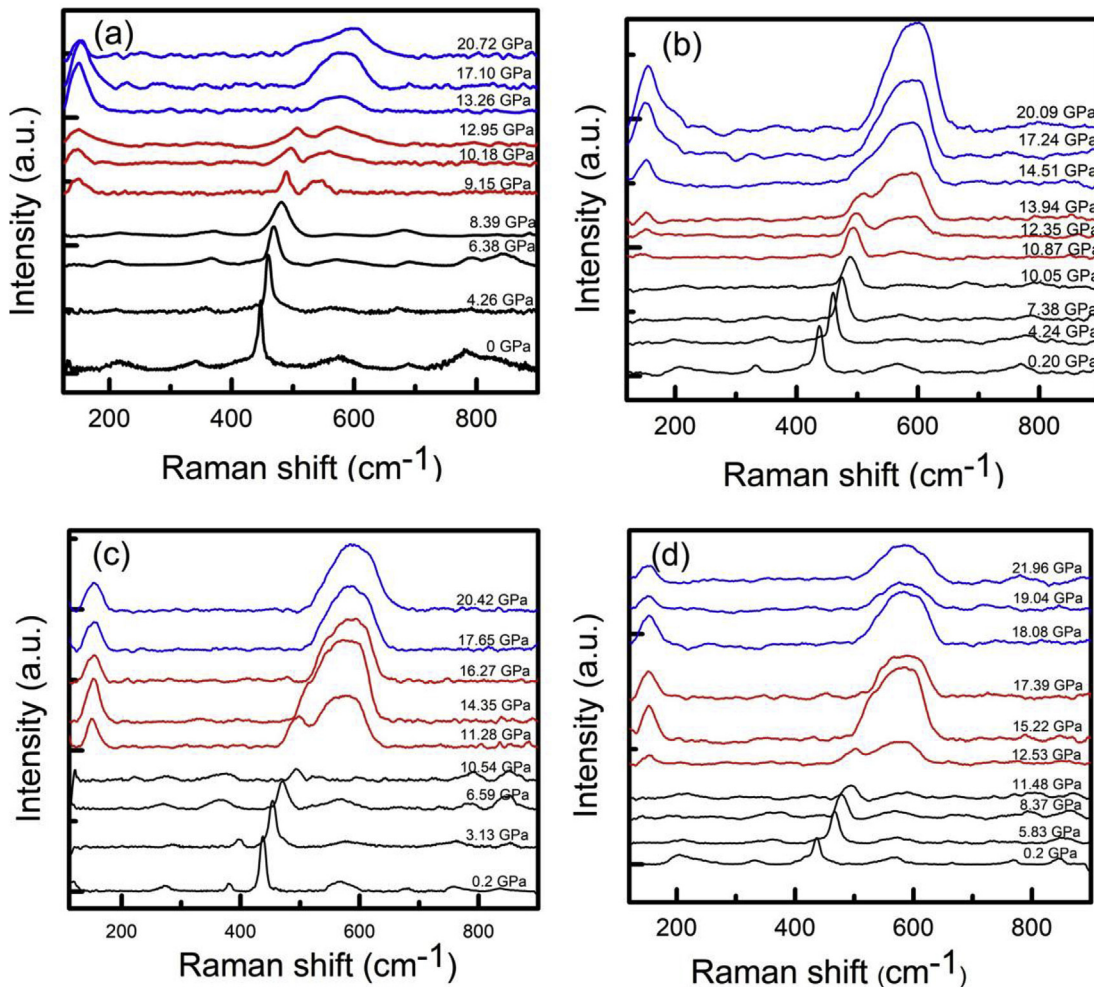


Fig. 7. Raman scattering at different pressures for (a) ZnO, (b) Zn_{0.95}Li_{0.05}O, (c) Zn_{0.95}Na_{0.05}O and (d) Zn_{0.95}K_{0.05}O samples: black plots: wurtzite phase; red plots: mixed phase; blue plots: rock salt phase. (For interpretation of the references to colour in this figure legend, the reader is referred to the Web version of this article.)

disappear.

3.4. High-pressure resistivity

Fig. 9(a) shows the electrical resistance measurements of pure ZnO nanoparticles as a function of pressure at room temperature. As the applied pressure increases, the resistance increases sharply and reaches its maximum at 9.34 GPa, when the structural phase

transition occurs. In general, the resistivity change in semiconductor materials under high pressure mainly arises due to a band gap change, which influences the number of electrons in the conduction band and holes in the valence band. Sans et al. [35] reported the pressure effect on the optical-absorption edge of a wurtzite ZnO sample. They observed a monotonic shift in the absorption edge towards higher energy as external high pressure increased. Therefore, the increase in electrical resistivity with

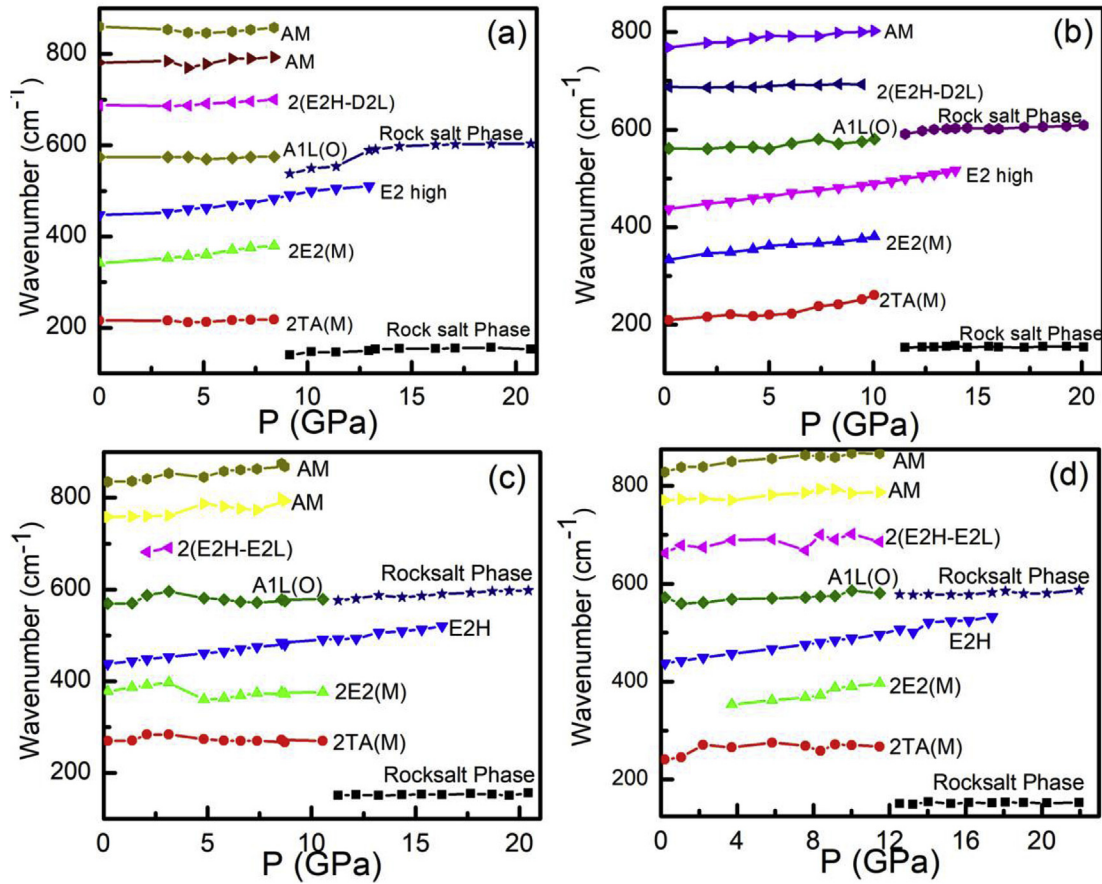


Fig. 8. Pressure dependence of the Raman peaks at different pressures for the (a) ZnO, (b) Zn_{0.95}Li_{0.05}O, (c) Zn_{0.95}Na_{0.05}O, and (d) Zn_{0.95}K_{0.05}O samples.

Table 3

Transition pressure values derived from Raman scattering for the start of the rock salt cubic phase, mixed phase region, and end of the wurtzite phase for ZnO, Zn_{0.95}Li_{0.05}O, Zn_{0.95}Na_{0.05}O, and Zn_{0.95}K_{0.05}O.

Samples	Pure wurtzite phase	Start of rock salt cubic phase - end of wurtzite phase (mixed phase)	Pure rock salt cubic phase
ZnO	8.39 GPa	9.15–12.95 GPa	13.26 GPa
Zn _{0.95} Li _{0.05} O	10.05 GPa	10.87–13.94 GPa	14.51 GPa
Zn _{0.95} Na _{0.05} O	10.54 GPa	11.28–16.27 GPa	17.65 GPa
Zn _{0.95} K _{0.05} O	11.48 GPa	12.53–17.39 GPa	18.08 GPa

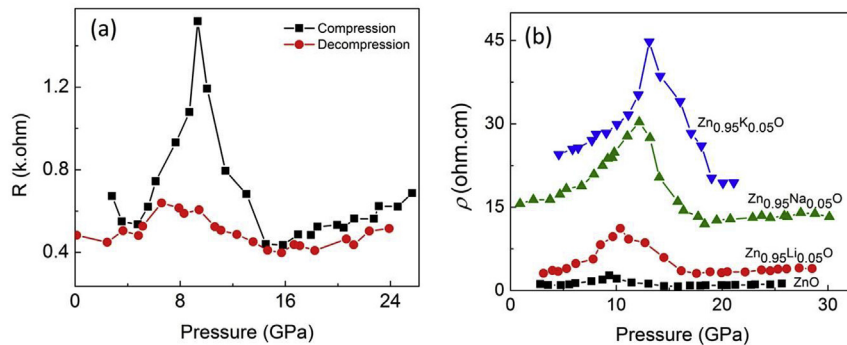


Fig. 9. (a) Resistance of pure ZnO particles vs. applied pressure during compression and decompression at room temperature; (b) Resistivities of pure, Li-, Na-, and K-doped ZnO particles vs. applied pressure during compression at room temperature.

applied pressure observed in our samples was due to band gap widening. Between 9.34 GPa and 14.52 GPa, we observed a mixture of wurtzite and rock salt phases and the resistance dropped from

the maximum value. During the transformation of the wurtzite to rock salt phase in pure ZnO, the coordination number changed from 4 to 6. Wickham et al. [36] discussed that the mechanism of

stacking disorder creation and destruction leads to atom plane sliding in the fourfold coordinated phase, which changes the electron density or crystal conductivity. Our electrical resistivity measurement directly reflects that the variation in the electron state is related to atomic structural variation under pressure, and hence, the transition pressure is related to a structural transition. By increasing pressure above the transition pressure, the resistivity started to increase slightly again. During decompression, the highest resistivity was observed at 6.03 GPa *i.e.*, ZnO reverted to a wurtzite structure. Generally, hysteresis relates to the presence of a structural transition due to externally applied pressure. When compared to compression, the structural transition upon decompression happens at a lower pressure. The original nanosize particles of the sample compressed together and formed a compact bulk, which may result in a decrease of electrical resistivity during decompression.

In order to compare the 1st group elements doping effect, the electrical resistivity of all 1st group element-doped ZnO samples were taken after considering their geometrical dimensions, and the results are shown in Fig. 9(b). Under pressure, the electrical resistivity increases with the ionic radius of the doping elements in ZnO, and the peak resistivity pressure shifts with the transition pressure, *i.e.*, the bigger the doping elements radius, the higher the resistivity value and transition pressure. Here, we observed two scenarios where resistivity increased with doping. First, the 1st group elements acted as acceptor dopants in the ZnO lattice, the divalent Zn ions were replaced by monovalent ions such as Li, Na, and K ions, and then holes were created, which were compensated by the electrons arising from the Zn²⁺ interstitials in the prepared ZnO. The hole concentration at the anion site increased, and the total density of states (DOS) at the Fermi level and the exchange interaction became smaller. Thus, the 1st group element-induced acceptor state was strongly localized within the gap region. This localization reduced the acceptor mobility [29]. Second, the lattice defects occurred in the prepared nanoparticles because of 1st group element incorporation into the ZnO lattice, reaction process and sintering. The lattice defects, such as the Zn interstitials and oxygen vacancy, played a vital role in the resistivity of prepared samples. The oxygen vacancy acted as a trap centre, and the delocalized electrons recombined with the oxygen vacancy defects. The charge mobility of the prepared samples decreased due to the presence of lattice defects [37].

4. Conclusion

In 1st group element-doped ZnO, doping elements such as Li, Na, and K occupied the Zn interstitial sites rather than the substitutional sites. Thus, doping Na and K in ZnO induced lattice strain, and tuned the Zn–O bond lengths due to their larger ionic radii. During the application of pressure, the crystalline size decreased due to the compression pressure, and subsequently, the lattice strain increased for all the samples. As a result, doping-induced lattice strain was hindered upon compression; the larger ions, rather than the smaller ions, tried to counteract the high pressure, due to ionic force repulsion within the lattice. As such, the disappearance of the wurtzite phase was also delayed to the high-pressure range. Here, the critical pressure of the cubic phase appearance increased from ~9 GPa to ~13 GPa from the pure to K-doped ZnO samples, respectively. The wurtzite phase stabilized more due to the increased monovalent ion size and the pressure required for the phase

transition enhanced further.

Acknowledgments

This work was financially supported by the National Nature Science Foundation of China (Grant No. U1530402, 51527801). HPCAT operations are supported by DOE-NNSA under Award No. DE-NA0001974 and DOE-BES under Award No. DE-FG02-99ER45775, with partial instrumentation funding by NSF. The gas loading was performed at GeoSoilEnviroCARS, APS, ANL, supported by EAR-1128799 and DE-FG02-94ER14466. APS is supported by DOE-BES, under Contract No. DE-AC02-06CH11357.

References

- [1] U. Ozgur, Ya. Alivov, C. Liu, A. Teke, M.A. Reshchikov, S. Doğan, V. Avrutin, S.J. Cho, H. Morkoc, *J. Appl. Phys.* 98 (2005), 041301.
- [2] A.P. Alivisatos, *Science* 271 (1996) 933.
- [3] S.H. Tolbert, A.P. Alivisatos, *Annu. Rev. Phys. Chem.* 46 (1995) 595.
- [4] S.H. Tolbert, A.P. Alivisatos, *Science* 265 (1994) 373.
- [5] P.F. Millan, *Nat. Mater.* 1 (2002) 19.
- [6] Z.W. Wang, *Proc. Natl. Acad. Sci. U. S. A.* 101 (2004) 13699.
- [7] R.Z. Valiev, Y. Estrin, Z. Horita, T.G. Langdon, M.J. Zehetbauer, Y.T. Zhu, *JOM J. Min. Met. Mat. S.* 58 (2006) 33.
- [8] C.C. Chen, A.B. Herhold, C.S. Johnson, A.P. Alivisatos, *Science* 276 (1997) 398.
- [9] F. Huang, J.F. Banfield, *J. Am. Chem. Soc.* 127 (12) (2005) 4523.
- [10] M.A. Meyer, A. Mishra, D.J. Benson, *Prog. Mater. Sci.* 51 (2006) 427.
- [11] A.M. Saitta, F. Decremps, *Phys. Rev. B* 70 (2004) 035214.
- [12] S.E. Boulfelfel, S. Leoni, *Phys. Rev. B* 78 (2008), 125204.
- [13] K. Keiji, S. Yasuhiko, K. Takumi, *Proc. Jpn. Acad. Ser. B* 75 (1999) 1.
- [14] Ravhi S. Kumar, A.L. Cornelius, M.F. Nicol, *Curr. Appl. Phys.* 7 (2007) 135.
- [15] F.J. Manjon, K. Syassen, R. Lauck, *High Pres. Res.* 22 (2002) 299.
- [16] Z. Dong, K.K. Stephen, A. Morin, L. Li, S. Jin, Y. Song, *J. Phys. Chem. C* 116 (2012) 2102.
- [17] S.J. Chen, Y.C. Liu, C.L. Shao, C.S. Xu, Y.X. Liu, L. Wang, B.B. Liu, G.T. Zou, *J. Appl. Phys.* 98 (2005), 106106.
- [18] S.J. Chen, Y.C. Liu, C.L. Shao, C.S. Xu, Y.X. Liu, L. Wang, B.B. Liu, G.T. Zou, *J. Appl. Phys.* 99 (2006), 066102.
- [19] C. Yu, Q. Yu, C. Gao, H. Yang, B. Liu, G. Peng, Y. Han, D. Zhang, X. Cui, C. Liu, Y. Wang, B. Wu, C. He, X. Huang, G. Zou, *J. Appl. Phys.* 103 (2008), 114901.
- [20] S.H. Tolbert, A.P. Alivisatos, *J. Chem. Phys.* 102 (1995) 4642.
- [21] S.H. Tolbert, A.B. Herhold, L.E. Brus, A.P. Alivisatos, *Phys. Rev. Lett.* 76 (1996) 4384.
- [22] S.B. Qadri, J. Yang, B.R. Ratna, E.F. Skelton, J.Z. Hu, *Appl. Phys. Lett.* 69 (1996) 2205.
- [23] J.Z. Jiang, L. Gerward, D. Frost, R. Secco, J. Peyronneau, J.S. Olsen, *J. Appl. Phys.* 86 (1996) 6608.
- [24] J.Z. Jiang, J.S. Olsen, L. Gerward, S. Morup, *Euro. Phys. Lett.* 44 (1998) 620.
- [25] Y. Wang, Y. Zhang, W.J. Chang, G.L. Lu, J.Z. Jiang, Y.C. Li, J. Liu, T.D. Hu, *J. Phys. Chem. Solid.* 66 (2005) 1775.
- [26] C.M. Lin, K.L. Lin, Y.K. Chern, C.H. Hsu, H.S. Sheu, Y.F. Liao, Y.W. Suen, S.R. Jian, J.Y. Juang, *J. Alloys Compd.* 604 (2014) 298.
- [27] A. Bouibes, A. Zaoui, *Solid State Commun.* 220 (2015) 36.
- [28] V. Pazhanivelu, A. Paul Blessington Selvadurai, R. Muruguraj, *Mater. Lett.* 151 (2015) 112.
- [29] Yanya Wei, Hou Denglu, Qiao Shuang, Zhen Congmian, Tang Guide, *Physica B* 404 (2009) 2486.
- [30] A.C. Larson, R.B.V. Dreele, Los Alamos National Laboratory Report LAUR, vol. 86, 2004.
- [31] P. Thompson, D.E. Cox, J.B. Hastings, *J. Appl. Crystallogr.* 20 (1987) 79.
- [32] H.K. Mao, J. Xu, P.M. Bell, *J. Geophys. Res.* 91 (1986) 4673.
- [33] (a) Nam-Hee Park, Yifeng Wang, Won-Seon Seo, Feng Dang, Chunlei Wan, Kunihito Koumoto, *Cryst. Eng. Comm.* 15 (2013) 679;
(b) Rik S. Koster, Changming M. Fang, Marjolein Dijkstra, Alfons van Blaaderen, Marijn A. van Huis, *J. Phys. Chem. C* 119 (10) (2015) 5648.
- [34] Xiaoqin Yan, Yousong Gu, Xiaomei Zhang, Huang Yunhua, Qi Junjie, Yue Zhang, Takeshi Fujita, Chen Mingwei, *J. Phys. Chem. C* 113 (2009) 1164.
- [35] J.A. Sans, A. Segura, F.J. Manjon, B. Mari, A. Munoz, M.J. Herrera-Cabrera, *Microelectron. J.* 36 (2006) 928.
- [36] J.N. Wickham, A.B. Herhold, A.P. Alivisatos, *Phys. Rev. Lett.* 84 (2000) 923.
- [37] Amir Zia, S. Ahmed, N.A. Shah, M. Anis-ur-Rehman, E.U. Khan, M. Basit, *Physica B* 473 (2015) 42.